



# A long-lived lunar dynamo powered by core crystallization



M. Laneuville<sup>a,\*</sup>, M.A. Wieczorek<sup>a</sup>, D. Breuer<sup>b</sup>, J. Aubert<sup>a</sup>, G. Morard<sup>c</sup>, T. Rückriemen<sup>b</sup>

<sup>a</sup> Institut de Physique du Globe de Paris, Sorbonne Paris Cité, Université Paris Diderot, Case 7011, 35 rue Hélène Brion, 75205 Paris Cedex 13, France

<sup>b</sup> Institute of Planetary Research, German Aerospace Center (DLR), 6 Rutherfordstraße 2, 12489 Berlin, Germany

<sup>c</sup> Institut de Minéralogie, de Physique des Matériaux, et de Cosmochimie (IMPIC), Sorbonne Universités – UPMC Univ Paris 06, UMR CNRS 7590, Muséum National d'Histoire Naturelle, IRD UMR 206, 4 Place Jussieu, F-75005 Paris, France

## ARTICLE INFO

### Article history:

Received 4 March 2014

Received in revised form 13 May 2014

Accepted 29 May 2014

Available online xxxx

Editor: Y. Ricard

### Keywords:

Moon

magnetic field

dynamo

core crystallization

paleomagnetism

## ABSTRACT

The Moon does not possess an internally generated magnetic field at the present day, but extensive evidence shows that such a field existed between at least 4.2 and 3.56 Ga ago. The existence of a metallic lunar core is now firmly established, and we investigate the influence of inner core growth on generating a lunar core dynamo. We couple the results of a 3-D spherical thermochemical convection model of the lunar mantle to a 1-D thermodynamic model of its core. The energy and entropy budget of the core are computed to determine the inner core growth rate and its efficiency to power a dynamo. Sulfur is considered to be the main alloying element and we investigate how different sulfur abundances and initial core temperatures affect the model outcomes. For reasonable initial conditions, a solid inner core between 100 and 200 km is always produced. During its growth, a surface magnetic field of about 0.3  $\mu\text{T}$  is generated and is predicted to last several billion years. Though most simulations predict the existence of a core dynamo at the present day, one way to stop magnetic field generation when the inner core is growing is by a transition between a bottom-up and top-down core crystallization scheme when the sulfur content becomes high enough in the outer core. According to this hypothesis, a model with about 6 to 8 wt.% sulfur in the core would produce a 120–160 km inner core and explain the timing of the lunar dynamo as constrained by paleomagnetic data.

© 2014 Elsevier B.V. All rights reserved.

## 1. Introduction

The Moon does not possess an active magnetic field today, but magnetic anomalies originating from its crust are observed at its surface (Purucker and Nicholas, 2010; Tsunakawa et al., 2010; Hood et al., 2013) and some samples returned from the surface possess a natural remanent magnetization (Dyal et al., 1970). Paleomagnetic studies dating from the Apollo era suggest a global field that lasted between 3.8 and 3.6 Ga ago (e.g., Cisowski et al., 1983), and furthermore, that the field strengths were as high as 100  $\mu\text{T}$  (Fuller and Cisowski, 1987 and references therein). For comparison, the present day field of the Earth is on the order of 50  $\mu\text{T}$ .

Lunar rocks are poor magnetic recorders and their thermal histories are often uncertain, therefore many of the Apollo era estimates should be used with caution (Lawrence et al., 2008; Tikoo et al., 2012a). Nevertheless, the current view suggests that a magnetic field of several tens of  $\mu\text{T}$  was present at the surface of the Moon between 4.2 and 3.56 Ga ago (Garrick-Bethell et al., 2009;

Shea et al., 2012; Tikoo et al., 2012a; Suavet et al., 2013). The lack of data before 4.2 Ga ago implies that the dynamo could be older, and there is also no definitive proof that the dynamo shut down 3.56 billion years ago, only that the surface magnetic field beyond that time was weaker (Tikoo et al., 2012b). Although there is no observed dynamo today, recent studies appear to indicate that a sample younger than 3.3 Ga, and maybe as young as  $\sim 1.3$  Ga (Fagan et al., 2013), acquired its primary magnetization from a dynamo field (Tikoo et al., 2014).

The most plausible mechanism for generating long lasting planetary magnetic fields is a core dynamo (Stevenson et al., 1983). Global planetary magnetic fields in terrestrial planets are generated by convection in their liquid outer cores. When more heat is extracted from the core than can be conducted along the adiabat, motion is triggered by thermal instabilities. The strength of the magnetic field is governed by the vigor of convection and the thickness of the convecting shell. However, the Moon is a small body and previous mantle thermal evolution studies found that heat extraction from the core is not large enough to produce a magnetic field for more than a few hundred million years, which is about ten times too short when compared to the paleomagnetic results (Konrad and Spohn, 1997; Laneuville et al., 2013). Models

\* Corresponding author.

E-mail address: laneuville@ipgp.fr (M. Laneuville).

with an initially stratified mantle, where KREEP- and ilmenite-rich magma ocean cumulates surrounded the lunar core, were able to produce a thermally induced core dynamo between 4.1 and 3.5 Ga ago (Stegman et al., 2003; Zhang et al., 2013). However, though this timing is marginally consistent with current observations, the lack of a KREEP signature in the titanium-rich mare basalts is potentially inconsistent with the underlying assumptions of this model. A recent study by Evans et al. (in press) proposed that the existence of a wet and initially stratified mantle could prolong the magnetic field era, but did not explicitly account for the history of mare volcanism.

It has been proposed that a lunar dynamo could also have been driven by differential rotation between mantle and core, induced either by precession of the mantle spin axis (Dwyer et al., 2011) or by changes in the rotation rate of the solid mantle following large impacts (Le Bars et al., 2011). In both cases, differential rotation induces large-scale flow in the core, which could have powered a lunar dynamo. The precession induced magnetic field is predicted to last from about 4.2–2.7 Ga ago with intensities of about 1  $\mu$ T, but may have troubles explaining paleomagnetic data outside of this range as new studies are published. The impact scenario predicts the existence of a magnetic field lasting about 10 thousand years. This could explain the existence of magnetic anomalies associated with the interiors of large impact basins, but cannot explain a dynamo field younger than the Orientale impact at about 3.7 Ga. We note here that it is unclear whether the efficiency and magnetic properties of such dynamos are similar to standard thermo/chemical ones.

As an alternative to previously proposed models, we study the influence of inner core growth on dynamo generation. This scenario has been studied in the case of the terrestrial planets (e.g., Stevenson et al., 1983) and asteroids (Nimmo, 2009), but has to date never been proposed for the Moon. In this model, compositional buoyancy due to the release of light elements at the inner core boundary helps to sustain convection in the outer core against dissipation, even when the heat extracted by the mantle is smaller than what could be conducted along the core's adiabat. This hypothesis has not been tested for the Moon before, in part because the bare existence of a lunar core – let alone an inner core – was debated (e.g., Wiczorek et al., 2006). A range of datasets has been used to constrain the lunar core size and state (including seismic analyses), and its radius is believed to lie between 250 and 450 km (Garcia et al., 2011; Weber et al., 2011) with at least some portion being partially molten at the present time (Williams et al., 2001). Recent lunar thermal evolution studies (Laneuville et al., 2013; Zhang et al., 2013) have suggested that core crystallization should indeed occur, and we therefore investigate this process in more detail in this study. We start by presenting our model in Section 2, which includes the coupling of a core energetics model to a 3-D mantle thermal evolution model. The predictions of our model are presented in Section 3, and we discuss some of the implications of this model in Section 4.

## 2. Lunar core evolution and magnetic field scaling

In order to estimate the strength of the surface magnetic field, the power available to drive the dynamo has to be estimated (Christensen and Aubert, 2006; Aubert et al., 2009). This power is directly linked to the sum of the thermal and chemical buoyancy forces within the core. As core and mantle evolution are coupled, we first need to model the thermal evolution of the mantle. The growth of the inner core is then obtained through the core energy budget, which is coupled to the bottom boundary condition of the mantle. Finally, we use the entropy budget to determine the part of the power available to dynamo action and a scaling law to

**Table 1**

Parameters used for the mantle thermal evolution simulations (see Laneuville et al., 2013).

| Symbol              | Description                   | Value   |
|---------------------|-------------------------------|---|
| $R_p$               | Moon radius                   | 1740 km   |
| $R_c$               | Core radius                   | 330 km  |
| $D_c$               | Crustal thickness             | 40 km   |
| $\Omega_K$          | PKT angular radius            | 40°   |
| $D_K$               | KREEP layer thickness in PKT  | 10 km   |
| $T_{\text{surf}}$   | Surface temperature           | 250 K   |
| $T_0$               | Reference temperature         | 1600 K  |
| $\eta_0$            | Reference viscosity           | 10 <sup>21</sup> Pa s                           |
| $\eta_{\text{max}}$ | Maximum viscosity             | 10 <sup>28</sup> Pa s                           |
| $E$                 | Activation energy             | 3 × 10 <sup>5</sup> J mol <sup>-1</sup>         |
| $L$                 | Mantle latent heat of melting | 6 × 10 <sup>5</sup> J kg <sup>-1</sup>          |
| $c_{p,m}$           | Mantle specific heat capacity | 1000 J kg <sup>-1</sup> K <sup>-1</sup>         |
| $k_c$               | Crust thermal conductivity    | 1.5 W m <sup>-1</sup> K <sup>-1</sup>           |
| $k_m$               | Mantle thermal conductivity   | 3 W m <sup>-1</sup> K <sup>-1</sup>             |
| $\kappa_0$          | Reference thermal diffusivity | 10 <sup>-6</sup> m <sup>2</sup> s <sup>-1</sup> |
| $\rho_0$            | Reference density             | 3400 kg m <sup>-3</sup>                         |
| $\alpha_{0,m}$      | Thermal expansivity           | 2 × 10 <sup>-5</sup> K <sup>-1</sup>            |
| $g$                 | Surface gravity acceleration  | 1.62 m s <sup>-2</sup>                          |

relate the magnetic field strength and power available from core convection.

We model the thermal evolution of the Moon using the Gaia 3-D thermochemical convection code with a temperature-dependent viscosity in a spherical shell (Hüttig and Stemmer, 2008). We follow closely Laneuville et al. (2013) and consider both core cooling and time-dependent radioactive decay of heat sources. We solve the conservation equations of mass, momentum and energy for an incompressible fluid under the Boussinesq assumption, with free-slip boundary conditions at both the surface and core mantle boundary. The consumption of latent heat through melting is taken into account assuming a peridotitic mantle. Mantle depletion from melting also adds a buoyancy source, which is then monitored by tracer particles, varying by 60 kg m<sup>-3</sup> between 0 and 30% depletion (the latter corresponding to harzburgite). However, heat source partitioning through mantle depletion is not considered. The rheology is Newtonian with a reference viscosity of 10<sup>21</sup> Pa s at 1600 K, corresponding to a dry mantle. Gravity is assumed constant throughout the mantle, which somewhat overestimates the buoyancy sources in the lower mantle. A table with relevant parameters for the mantle thermal evolution simulations can be found in Table 1. For a complete description of the model, as well as discussion about possible limitations to the model, the reader is referred to Laneuville et al. (2013).

A 1-D geometry is used to model the core because we are interested only in its long-term, averaged evolution rather than in the short-term perturbations associated with core convection. We ignore explicitly any potential complications that may arise due to a non-uniform core mantle boundary heat flow (Glatzmaier et al., 1999; Takahashi and Tsunakawa, 2009). Fig. 1 is a schematic of our core model, showing the core temperature profile and the liquidus temperature in the outer core. The liquid outer core is assumed to be well-mixed, and thus to follow an adiabatic temperature profile. This approximation is not valid when core convection is not occurring, such as after the termination of an initial thermal dynamo stage and before the onset of core crystallization. Nevertheless, this should affect only the time at which core crystallization occurs by a few 100 million years. The solid inner core is assumed to be isothermal due to its high thermal conductivity.

The inner core size is computed by comparing the adiabatic temperature profile in the liquid core to the liquidus of the iron alloy. As the inner core grows, the outer core becomes enriched in sulfur and the liquidus temperature decreases. A simple mass balance provides  $\chi(r_i) = \chi_0 / (1 - f^3)$ , where  $\chi_0$  and  $\chi$  are the sulfur mass fraction in the core initially and as a function of in-

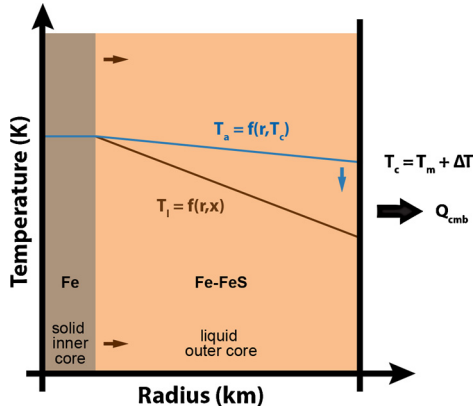


**Fig. 1.** Schematic 1-D model of the core. The inner core is isothermal and its size is defined by the intersection point of the adiabat and the liquidus (which depends upon composition).  $T_c$  is the temperature at the top of the core, which is initially superheated by  $\Delta T$  with respect to the initial mantle temperature  $T_m$ . The heat flow out of the core is determined by the mantle thermal evolution, and the adiabatic temperature profile depends upon radius and the temperature of the core-mantle boundary. As core cooling proceeds, the adiabatic temperature profile shifts downwards, causing core crystallization.

ner core radius  $r_i$ , and where the ratio of inner core to outer core radius  $r_i/R_c$  is denoted  $f$ . We note here that the effect of partitioning is relatively small, as an inner core radius of about 80% is required before doubling the initial sulfur concentration in the outer core. Sulfur will be considered as the primary alloying element, and discuss the specificities of other light elements at the end of this section. Fig. 1 is a schematic of our core model, showing the core temperature profile and the liquidus temperature in the outer core.

In the absence of core crystallization, the core energy budget contains only secular cooling. But when the inner core starts to freeze, two energy sources appear: latent heat release and a chemical buoyancy source. Assuming that no radioactive heat sources are present in the core, and that the core is in instantaneous thermal equilibrium with the lowermost mantle, the energy budget can be written as

$$Q_{CMB} = Q_S + Q_L + Q_g, \quad (1)$$

where  $Q_{CMB}$  is the average heat flux out of the core, and  $Q_S$ ,  $Q_L$  and  $Q_g$  are the parts of the core mantle boundary heat flow due to secular cooling of the core, latent heat release upon inner core growth and dissipated heat from compositional buoyancy due to sulfur concentration in the remaining fluid, respectively. The left-hand side is calculated from the mantle thermal evolution model and the right side of this equation will be used to determine how the core temperature changes for a given amount of heat extracted by the mantle. For an isentropic outer core with homogeneous composition, the temperature profile is adiabatic and can be approximated by Labrosse (2003)

$$T_a(r, T_c) = T_c \exp\left[-\frac{r^2 - R_c^2}{D^2}\right], \quad (2)$$

where  $r$  is radius,  $T_c$  the temperature at the core-mantle boundary,  $R_c$  the core radius and  $D$  the adiabatic scale height

$$D = \left(\frac{3c_{p,c}}{2\pi\alpha\rho_{oc}G}\right)^{1/2}, \quad (3)$$

where  $G$  is the gravitational constant,  $\rho_{oc}$  the outer core density,  $c_{p,c}$  the core heat capacity and  $\alpha$  the thermal expansivity. Thermal boundary layers do not alter the thermal structure in the core.

Assuming an adiabatic temperature profile for the outer core and an isothermal inner core implies that the complete core state

is determined by one temperature only, which we choose to be the core-mantle boundary temperature. This temperature is initially set to be equal to the temperature in the lower mantle, overheated by  $\Delta T$  to account for residual heat of differentiation. The inner core growth is therefore directly proportional to the core-mantle boundary temperature evolution and can be obtained through the intersection of the liquidus and adiabatic temperature at the inner-core boundary. After the core cools by  $\delta T_c$ , the adiabat and liquidus temperature at  $r = r_i + \delta r_i$  are equal, which can be written as

$$T_l(r_i + \delta r_i) = T_a(r_i + \delta r_i, T_c - \delta T_c). \quad (4)$$

From a first order Taylor expansion of both sides of this equation, in which we neglect the partial derivative of the liquidus with respect to composition and assume hydrostatic equilibrium (i.e.,  $dP = \rho_{ic}g(z)dz$ ), we obtain

$$\frac{dr_i}{dt} = \frac{1}{(dT_l/dP - dT_a/dP)\rho_{ic}g} \frac{T_i}{T_c} \frac{dT_c}{dt}, \quad (5)$$

where  $\rho_{ic}$  is the inner core density,  $T_i$  is the temperature at the inner core boundary,  $g$  the gravity acceleration at the inner core boundary, and  $dT_l/dP$  and  $dT_a/dP$  are the change of melting temperature and adiabatic gradient with pressure, respectively. Neglecting the partial derivative with respect to composition leads to a small error in inner core growth rate when the inner core is small, which only becomes significant when the inner core reaches about 0.6  $R_c$ . Assuming  $T_i \sim T_c$  and  $dT_a/dr = -2rT_c/D^2$ , Eq. (5) can be further simplified to

$$r_i \frac{dr_i}{dt} = \frac{D^2}{2T_c(\Delta - 1)} \frac{dT_c}{dt}, \quad (6)$$

where  $\Delta = (dT_l/dP)/(dT_a/dP)$  (Nimmo, 2009). This assumption leads to an error in inner core growth rate of less than 1%.

The secular cooling term takes into account the heat released as the core cools. We use a second order Taylor expansion of Eq. (2) in  $(R_c/D)$  to obtain

$$Q_S = M_c c_{p,c} \left(1 + \frac{2R_c^2}{5D^2}\right) \frac{dT_c}{dt}, \quad (7)$$

where  $M_c$  is the total mass of the core. The latent heat term corresponds to the heat released as the inner core solidifies and can be written as

$$Q_L = \frac{3}{2} M_c \frac{fL_H}{T_c} \frac{D^2}{R_c^2} \frac{1}{\Delta - 1} \frac{dT_c}{dt}, \quad (8)$$

where  $L_H$  is the latent heat of crystallization. Finally, the compositional buoyancy contribution corresponds to the change in potential gravitational energy due to the release of light elements at the inner core boundary (i.e., growth of a dense inner core). It can be written as

$$Q_g = 3\pi G \rho M_c F \frac{\Delta\rho_c}{\rho_{ic}} \frac{1}{\Delta - 1} \frac{D^2}{T_c} \frac{dT_c}{dt}, \quad (9)$$

where  $F = f(1/5 + 2f^5/15 - f^2/3)/(1 - f^3)$ , and  $\Delta\rho/\rho_{ic}$  is the relative density change upon inner core solidification with  $\Delta\rho_c = \rho_{oc} - \rho_{ic}$ . The ratio  $(R_c/D)$  is about 0.1, thus a second order truncation of Eq. (2) creates an error of less than 0.01 K in the adiabatic temperature profile. To derive Eq. (9), we assumed that the density jump at the inner-core boundary gives rise to a negligibly small perturbation of the gravity potential. For a complete derivation of the heat flows, see Nimmo (2007, 2009). The set of Eqs. (6) and (7)–(9) can then be solved iteratively to obtain the evolution of the inner core size.

The energy budget only considers the total amount of heat that leaves the core. Magnetic energy is created and dissipated within

the core itself and therefore does not enter this global energy balance. Ohmic dissipation is, however, a non-reversible process and as such, doesn't conserve entropy. The existence of other entropy sinks reduce the amount of energy available in the system to drive the dynamo. Because the quantity of energy available is limited, the entropy budget can be used to estimate the amount of energy that can be dissipated by dynamo action. It is written as

$$E_\phi + E_k = E_s + E_g + E_L, \quad (10)$$

where  $E_\phi$  is the entropy sink due to dissipation,  $E_k$  is the entropy sink associated with conduction,  $E_s$  is the entropy production due to secular cooling,  $E_L$  is the entropy production due to latent heat release at the inner core boundary and  $E_g$  is the gravitational contribution associated with release of light elements at the inner core boundary. Other entropy producing sources, such as friction at the core mantle boundary between the liquid core and the mantle, could perhaps increase the amount of energy available to sustain the dynamo, but the additivity of the processes is unclear. For a stable dynamo to occur, enough entropy has to be produced to balance ohmic dissipation, that is,  $E_\phi$  has to be greater than zero. Starting from the local entropy conservation equation, which can be integrated over the core, one can identify the corresponding terms to Eq. (10) and obtain the expression of the different entropy contributions. The derivation of these terms can be found in Nimmo (2007) and they can be written as

$$E_s = M_c c_{p,c} \frac{2R_c^2}{5T_c D^2} \frac{dT_c}{dt}, \quad (11)$$

$$E_g = \frac{Q_g}{T_c}, \quad (12)$$

$$E_L = \frac{3}{2} M_c \frac{f(1-f^2)L_H}{T_c^2} \frac{1}{\Delta-1} \frac{dT_c}{dt}, \quad (13)$$

$$E_k = M_c \frac{12k}{5\rho_{oc} D^4} R_c^2, \quad (14)$$

where  $k$  is the core thermal conductivity.

Before inner core nucleation,  $E_g$  and  $E_L$  are both zero, but following inner core crystallization, they play an important role. The entropy production linked to latent heat release operates at a higher temperature than entropy production by secular cooling, and thus has an intrinsically higher efficiency factor of about 2.

The volumetric power available to drive the dynamo is the power that corresponds to  $E_\phi$ , which is

$$\Phi = \frac{E_\phi T_i}{V_{oc}}, \quad (15)$$

where  $V_{oc}$  the volume of the outer core. Using  $T_i$  as the temperature at which dissipation occurs means that we slightly overestimate the total amount but is consistent with the previous assumption that  $T_i \sim T_c$ .

In addition to constraints on the energy available to generate a dynamo, there are constraints on whether the fluid motion is able to power a dynamo. The magnetic Reynolds number characterizes the importance of magnetic advection in comparison to magnetic diffusion and is defined as  $Re_m = \nu L / \eta$ , where  $\nu$  is the characteristic velocity,  $L$  the characteristic length (taken to be the thickness of the convective shell) and  $\eta$  the magnetic diffusivity. In order for dynamo action to occur, the Reynolds number must be greater than a numerically defined critical value of about 40 (Christensen and Aubert, 2006). Following Nimmo (2009), we estimate the velocity induced by chemical buoyancy by

$$\nu \simeq 0.85 R_c^{3/5} \Omega^{-1/5} \left( \frac{4\pi G \Delta \rho}{3} \frac{dr_i}{dt} \right)^{2/5}, \quad (16)$$

where  $\Omega$  is the rotation rate. This approach is based on numerical experiments (Olson and Christensen, 2006) and assumes that most of the buoyancy flux comes from inner core growth. Using the present day rotation rate  $\Omega = 2\pi/27 \text{ days}^{-1}$  in order to obtain a conservative lower bound on  $\nu$ , a typical growth rate in our simulations of  $40 \text{ km Ga}^{-1}$  and  $\eta = 2 \text{ m}^2 \text{ s}^{-1}$ , we obtain a typical fluid velocity of about  $0.7 \text{ mm/s}$ . Thus  $Re_m \simeq 120$ , which is well above the critical value for dynamo activity. This confirms that, if the available energy for dissipation is positive, as defined in the previous section, a dynamo is likely to occur.

Once we obtain the volumetric energy available for the dynamo, we can use a magnetic field scaling law to estimate the average intensity of the surface magnetic field. Aubert et al. (2009) generated a scaling law that improved upon the earlier work of Christensen et al. (2008) by expanding the parameter space and by using a larger range of inner core sizes. Their study includes inner cores with radii up to  $0.35R_c$ . Models with inner cores larger than at least  $0.65R_c$  may reach the thin shell regime and would likely not follow this scaling law (Heimpel et al., 2005). Regardless, this does not happen in our case and we thus use the scaling law presented in Aubert et al. (2009), which is

$$B = f_e (\rho_{oc} \mu_0^3 \Phi^2 L^2)^{1/6} \left( \frac{R_c}{R_p} \right)^3, \quad (17)$$

where  $B$  is the average magnetic field strength at the surface of the Moon,  $\mu_0$  the permeability of free space,  $\Phi$  the volumetric power available for the dynamo as computed above,  $L$  is the outer core thickness  $R_c - r_i$ , and  $R_p$  the radius of the Moon. The prefactor  $f_e$  is an efficiency factor that includes a scaling law prefactor of order 1 and the ratio of magnetic field inside the shell to the dipole field just outside the CMB that is about 0.1. This factor exists because only about 1/2 of the energy is in the poloidal part external to the core and only a fraction of that energy is in the dipole term (the rest being in higher multipole terms). According to Aubert et al. (2009), these ratios are constant for a wide range of parameters, which includes this study. Note here that  $B \propto \Phi^{1/3}$ , which limits the increase in surface field strength with dissipation. An order of magnitude increase in  $B$  requires 3 orders of magnitude increase in  $\Phi$ .

We focus on the Fe–FeS system as it is the one with the most experimental data available. We use the melting temperature proposed by Buono and Walker (2011), which is of order 4 in pressure and composition. The main uncertainty on the core liquidus comes from the pressure-radius relationship. To first order, we consider the pressure decrease from the Moon's center as  $P(r) = P_0 - 2\pi r^2 \rho_{ic}^2 G / 3$ , where  $P_0$  is the central pressure. The value of  $P_0$  is model dependent and chose 5.1 GPa as our nominal value (Garcia et al., 2011, 2012).

The density of the solid inner core is assumed constant while the density of the outer core varies linearly with sulfur content (Nishida et al., 2008). The density of pure liquid and solid Fe at 4 GPa is taken from the equation of state presented in Komabayashi and Fei (2010), which give  $\rho_{oc} = 7.0 \text{ g/cm}^3$  and  $\rho_{ic} = 7.5 \text{ g/cm}^3$ , respectively.

A complete description of the Fe–FeS system would require a temperature and pressure dependent thermal expansivity that is also a function of sulfur content. However, considering some of the first order simplifications in the model and the fact that the reference thermal expansivity for liquid iron is still controversial (Williams, 2009), we use an average value at ambient pressure proposed in Williams (2009), and use the liquid iron equation of state to determine a typical value at lunar core conditions. This value is then kept constant in the thermal models. The equation of state is as follows:

$$\alpha = \alpha_{0,c}(T_{\text{ref}}) K_0(T_{\text{ref}}) / (K_0(T_{\text{ref}}) + K_p(P - P_{\text{ref}})), \quad (18)$$

where the isentropic bulk modulus  $K_0(T_{\text{ref}}) = 109.7$  GPa, the pressure derivative  $K_P = 4.66$ ,  $T_{\text{ref}} = 1811$  K and  $P_{\text{ref}} = 1$  bar (Anderson and Ahrens, 1994). These parameters lead to a value of  $\alpha = 9.2 \times 10^{-5} \text{ K}^{-1}$  at 5 GPa. A summary of the parameters we use can be found in Table 2.

Using carbon or silicon as alloying elements would produce a different core evolution as a result of their crystallizing behaviors. In the Fe–FeS system at lunar pressures, pure Fe is crystallizing whereas in the Fe–FeSi system the solid crystallizes with almost the same composition as the liquid. Only the latent heat contribution would exist in that case, and no compositional buoyancy would be released at the inner core boundary. This suggests that a dynamo could not be as easily sustained as compositional buoyancy is the main driver in the Fe–FeS system. In the Fe–Fe<sub>3</sub>C system, a mixture of Fe and C crystallizes while still enriching the outer core in C. We therefore expect that an Fe–Fe<sub>3</sub>C system would produce intermediate results, between that of S and Si. Recognizing the lack of data in these two systems, we investigate only the Fe–FeS system as it should give rise to the highest magnetic field strengths.

### 3. Model predictions

In the following subsections, we will first present a typical mantle and core thermal evolution and its main features. Then we will investigate the influence of initial sulfur content and the consequences this has on the evolution of the Moon's magnetic field.

#### 3.1. Typical evolution

The initial conditions in the mantle are the same for all runs of this study and follow Laneuville et al. (2013). The bulk silicate uranium content is 25.1 ppb. The potassium and thorium concentrations are given by the ratios  $K/U = 2500$  and  $Th/U = 3.7$ , respectively. About one third of the total heat source content is localized below the crust of the Procellarum KREEP Terrane, as suggested by the distribution of uranium, thorium and potassium obtained from  $\gamma$ -ray spectrometer observations of the surface (Lawrence et al., 1998). The initial temperature profile following magma ocean crystallization starts from a surface value of 250 K, is linear in the 40-km thick crust, and reaches the mantle solidus at the base of the crust. The profile then follows the solidus of peridotite for the first 350 km, corresponding to a region of the crystallized magma ocean that did not have time to gravitationally readjust. We also consider colder cases, where the profile follows the solidus only for the first 200 km, and we discuss the implications of these models in the next section. The lower mantle is set to an adiabatic profile and the initial temperature of the core is set to the mantle temperature overheated by an amount  $\Delta T$ , corresponding to residual heat from core differentiation. The core has a radius of 330 km.

Assuming that the gravitational energy difference upon core differentiation heats the core materials preferentially, an initial temperature excess of about 700 K could be observed (e.g., Solomon, 1979). Heat partitioning between iron and silicates during differentiation is not well constrained, and we thus consider extreme cases to assess the consequences of this effect. Following Konrad and Spohn (1997), we use a lower limit of 200 K, as well as the higher limit of 400 K as used in Laneuville et al. (2013). The case where the core has not been heated with respect to the mantle, and thus has an initial temperature equal to the core mantle boundary liquidus temperature will also be discussed. A complete study of the mantle thermal evolution following from these initial conditions is described in Laneuville et al. (2013).

Fig. 2 shows a slice of the temperature field for different times in a representative thermal evolution of the Moon from 4.5 Ga to the present day. As previously shown in Laneuville et al. (2013),

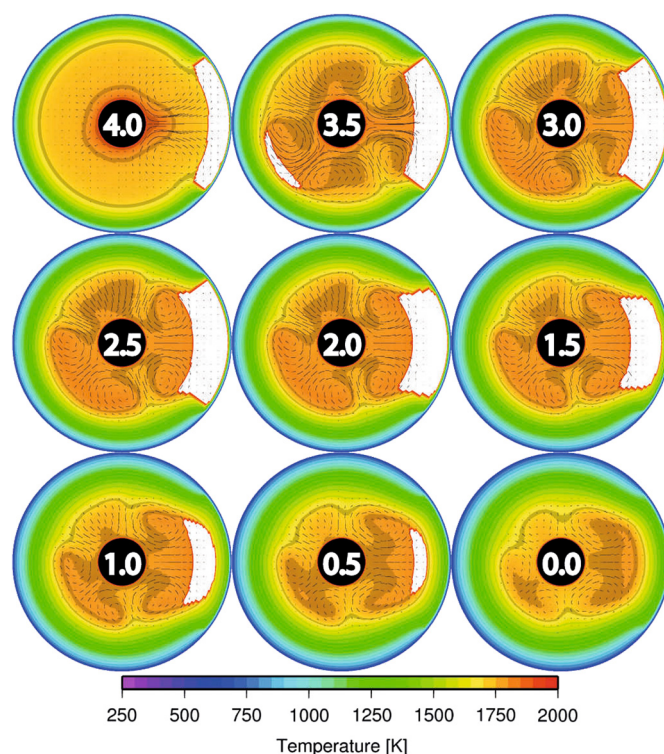


**Fig. 2.** Temperature cross sections of the lunar mantle for a complete thermal evolution, from 4.5 Ga ago to the present. Initial conditions corresponds to the nominal model of Laneuville et al. (2013). Numbers correspond to time before present in Ga. The central black circle is the lunar core and white corresponds to regions that are partially molten. Mantle streamlines are shown as dashed lines. (For interpretation of the colors in this figure, the reader is referred to the web version of this article.)

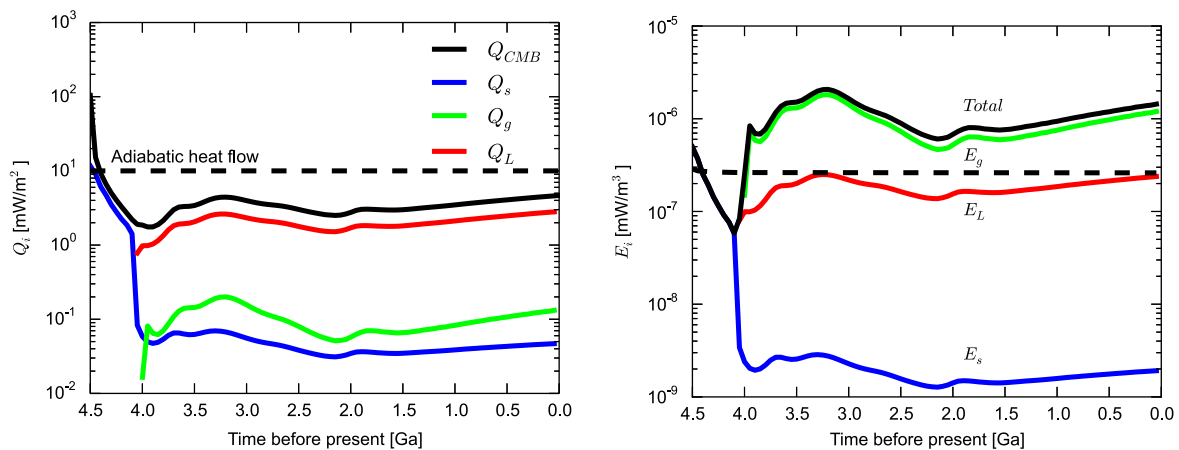
for simulations with most of the heat sources localized in the near-side crust, volcanism occurs mainly on the nearside, though small amounts of melting are still possible on the farside between 4 and 3.5 Ga ago. Because of the asymmetric initial conditions, the core-mantle boundary heat flow is slightly asymmetric as well, but the average value is independent of the exact heat sources distribution as long as they are located in the upper mantle.

Fig. 3a is an example of the different contributions to the core energy budget for the simulation shown in Fig. 2. For the first 200 million years, the heat flow is in excess of that conducted along the adiabat, allowing for thermal convection in the core. Before inner core nucleation at 4.0 Ga, the extracted heat contributes to secular cooling of the core only. As soon as inner core crystallization occurs, the release of latent heat accounts for most of the heat extracted from the core and there is a strong reduction in the core cooling rate. This is different than what is expected for the Earth, because the smaller pressure range on the Moon makes the liquidus less steep. This implies that the ratio of the latent heat released per cooling unit is much larger on the Moon than Earth. The influence of the compositional energy release at the inner core boundary on the energy budget is small compared to the influence of latent heat of crystallization.

Fig. 3b shows the different contributions to the entropy budget for the same simulation. The threshold that needs to be crossed in order to have convection and hence, dissipation is shown as a dotted black line, which represents the entropy sink rate associated with conduction along the adiabat. As soon as inner core crystallization occurs, the total entropy production rises above that threshold and thus, dynamo action is possible. The entropy production associated with the compositional term plays the largest role in the entropy budget. This happens because the associated energy is released directly in the form of buoyancy whereas the

**Table 2**  
Core evolution model parameters.

| Variable        | Value                 | Units                                | Reference                  |
|-----------------|-----------------------|--------------------------------------|----------------------------|
| $R_c$           | 330                   | km                                   | Weber et al. (2011)        |
| $c_{p,c}$       | 835                   | $\text{J kg}^{-1} \text{K}^{-1}$     | Nimmo (2009)               |
| $k$             | 50                    | $\text{W m}^{-1} \text{K}^{-1}$      | de Koker et al. (2012)     |
| $L_H$           | 300                   | $\text{kJ kg}^{-1}$                  | Stevenson et al. (1983)    |
| $P_0$           | 5.1                   | GPa                                  | Garcia et al. (2011)       |
| $\alpha_{0,c}$  | $1.12 \times 10^{-4}$ | $\text{K}^{-1}$                      | Williams (2009)            |
| $\rho_{ic}$     | 7.5                   | $\text{g cm}^{-3}$                   | Komabayashi and Fei (2010) |
| $\rho_{oc}$     | 7.0                   | $\text{g cm}^{-3}$                   | Komabayashi and Fei (2010) |
| $d\rho_1/d\chi$ | -0.4                  | $\text{g cm}^{-3} \text{wt.}\%^{-1}$ | Nishida et al. (2008)      |
| $K_0$           | 109.7                 | GPa                                  | Anderson and Ahrens (1994) |
| $K_p$           | 4.66                  | -                                    | Anderson and Ahrens (1994) |
| $D$             | 3046                  | km                                   | Eq. (3)                    |
| $f_e$           | 0.1                   | -                                    | -                          |



**Fig. 3.** Typical energy (left) and entropy (right) budget evolutions. The 's', 'L' and 'g' subscripts correspond to the secular, latent heat and compositional fractions of the budget, respectively. The dashed line in the energy budget corresponds to the heat flow conducted along the adiabat. The dashed line in the entropy budget corresponds to the threshold required to power a dynamo. The solid black line corresponds to the sum of the entropy sources. These budgets correspond to the case with  $\Delta T = 300 \text{ K}$  and  $\chi_0 = 6 \text{ wt.}\% \text{ S}$ .

other terms are released in the form of heat and have to undergo more transformations before leaving the system.

The outcome of two core evolution simulations are presented in Fig. 4. Both have an initial sulfur content of 4 wt.% and they differ by the initial difference in core temperature. The first important point to note is that once the inner core starts to grow (after  $\sim 100$  and  $\sim 500$  million years, respectively), the cooling rate of the core is dramatically reduced. The reason is that latent heat release upon crystallization becomes comparable to the total heat flow extracted, as shown in Fig. 3a, and thus acts as a buffer to core cooling. As a consequence, and because the lower mantle is cooling faster in the meantime, the core mantle boundary heat flow increases with time.

The initial temperature difference between core and mantle does not play a major role on the final evolution of the core. The only influence is on the early evolution: the hotter the core, the longer it takes to cool it down to the liquidus and start crystallizing. In this figure, the 100 K initial temperature difference leads to an almost 500 million year delay in the onset of inner core crystallization. However, the rest of the evolution is very similar, and the present day inner core sizes are nearly indistinguishable.

Fig. 4d shows the predicted surface magnetic field as a function of time. The thermally induced dynamo is present from the start of our simulations, but only lasts a few 100 million years. Then depending on the initial core mantle temperature difference, the compositionally induced dynamo starts somewhere between 4.4 and 4 Ga ago. The nearly constant growth rate of the inner core induces a nearly constant surface magnetic field at the surface for most of the lunar history. The field is on the order of  $0.3 \mu\text{T}$ ,

which is similar to other studies that have used similar magnetic field scaling relationships (Dwyer et al., 2011; Le Bars et al., 2011; Evans et al., in press). These intensities are an order of magnitude too small when compared to paleomagnetic intensities between about 4.2 and 3.56 Ga (which are several tens of  $\mu\text{T}$ ), but are consistent with a younger, low intensity dynamo as suggested by Tikoo et al. (2012b, 2014) (below a few  $\mu\text{T}$ ).

Finally, these typical cases predict the existence of a dynamo up to the present day. This is very important because it shows that if the Moon possess an inner core, then we should expect to observe a long lasting magnetic field. Other thermal evolution models, such as Zhang et al. (2013), also predict the growth of an inner core, and although they did not consider entropy production due to core crystallization as a source of energy to power a dynamo, their simulations should also produce a dynamo generated magnetic field up to the present day. This suggests that some process exists to shut off a dynamo driven by core crystallization.

### 3.2. Influence of initial core sulfur content

In this subsection, we present the influence of the initial sulfur content on core evolution. As observed earlier, the core temperature stays almost constant once the inner core starts to grow. Fig. 5a is a good way to visualize the liquidus dependence on sulfur content. With 2 wt.% initial sulfur content, the inner core starts to grow at about 1900 K, whereas for 8 wt.%, core crystallization commences at about 1760 K. The higher core temperature of the former case leads to a larger heat flow, which will in turn lower

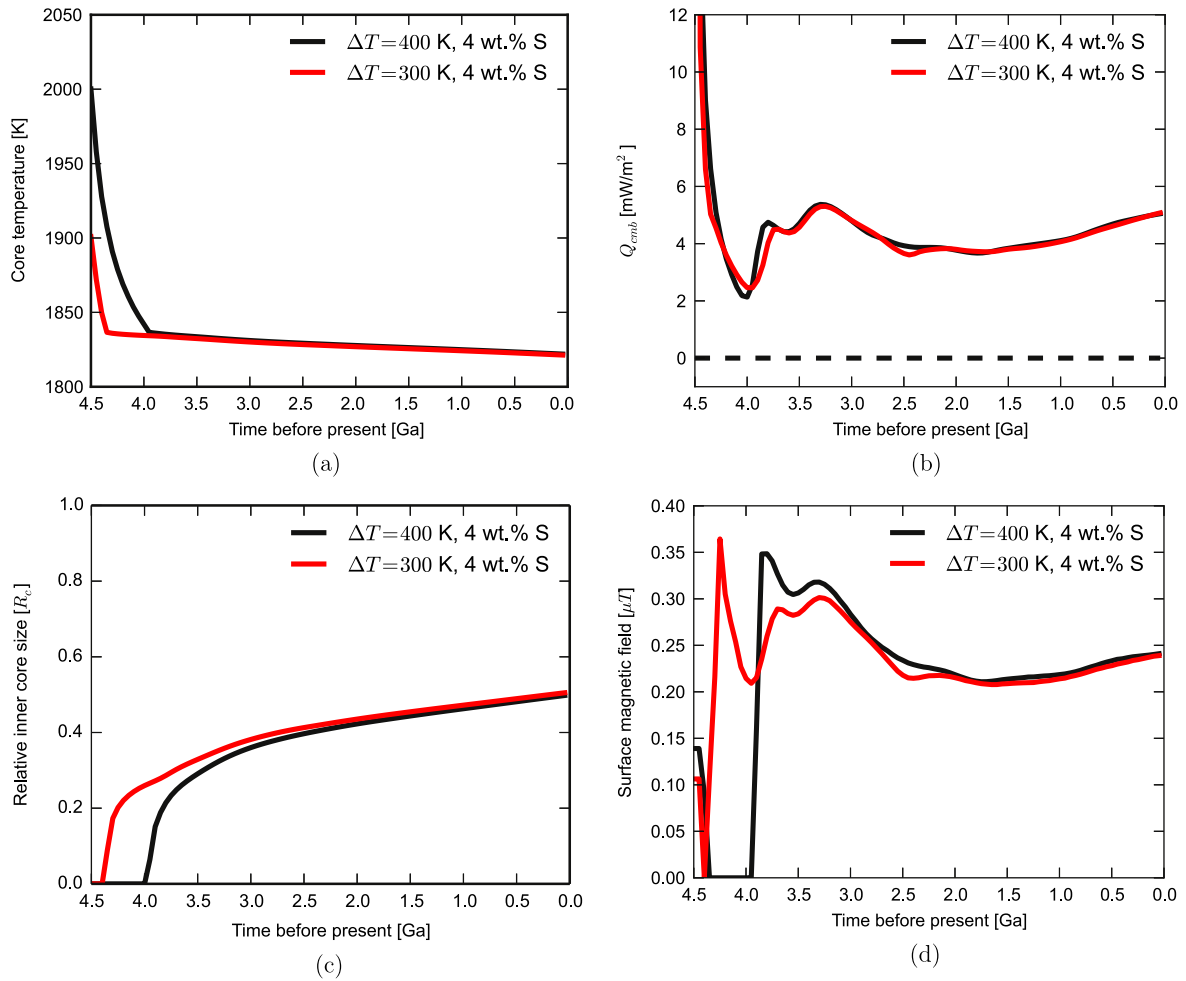


**Fig. 4.** Core evolution scenarios for two different values of the initial temperature difference between the core and mantle,  $\Delta T = 300$  and  $400$  K, for a sulfur content of 4 wt.%. From top left to bottom right: (a) core temperature as a function of time, (b) core-mantle boundary heat flow, (c) relative inner-core size and (d) predicted average surface magnetic field strength.

the viscosity at the base of the mantle and thus increase the cooling rate further.

All cases presented here have an inner core at the present day: the lower the sulfur content, the larger is the inner core at present day. The initial core mantle temperature difference only affects the onset of core crystallization and its associated magnetic field, and an important observation is that the present day inner core appears to be limited to the range of 0.3–0.6  $R_c$  in radius (i.e., 100–200 km). For sulfur contents higher than about 8 wt.%, the liquidus and adiabatic slope are almost equal and a top-down (i.e., Fe-snow) crystallization regime should be expected. Such a regime is not expected to be able to sustain dynamo activity for more than 100 million years (Rückriemen et al., 2014), and the probable transition will be discussed in the next section.

If we now look at the predicted surface magnetic field (Fig. 5d), we see that the general behavior is similar, whatever the initial sulfur content is. As the inner core starts to grow, a nearly constant magnetic field is observed for most of lunar history. The amplitude of the field varies only by about a factor of 4 among our models, and is related to sulfur content, both through the volumetric inner core growth rate and convective shell thickness (see Eq. (17)). We also observe that for an initial sulfur content of 8 wt.%, the dynamo is at the threshold of its existence, where chemical buoyancy is not always strong enough to overcome the stable thermal gradient. Because core-mantle boundary heat flow increases with time in the last 2 billion years of lunar history, our simulations predict the surface magnetic field strength will increase as well. It is therefore

improbable to find a case with a long lasting magnetic era between at least 4.2 and 3.3 Ga which then shuts off by itself before the present day.

#### 4. Discussion

Paleomagnetic studies show that the Moon possessed a global magnetic field between at least 4.2 and 3.56 Ga ago. However, the question of when the dynamo started and stopped remains unresolved. Thermal dynamos following lunar formation are very short lived, with lifetimes of a few 100 million years. The removal of an unstable thermal blanket around the core-mantle boundary (Zhang et al., 2013) could increase the lifetime of a thermal dynamo, but even in those cases, the dynamo is predicted to last no longer than 1 billion years. The precession-driven dynamo models make similar predictions and suggest a nominal extent of the dynamo period lasting until 2.7 Ga ago.

We have shown here that inner core growth is expected to sustain a dynamo that could have lasted up to the present day and with an onset between 4.5 and 4 Ga ago. As new paleomagnetic measurements are made outside of the 4.2–3.56 Ga ago time period, it will be possible to discriminate between these different classes of models. Indeed, the preliminary measurements of Tikoo et al. (2014) suggest that a young regolith breccia acquired its primary magnetization in a dynamo field. Its age is still ambiguous but it appears to be at most 3.3 Ga old, and may be as young as  $\sim 1.3$  Ga (Fagan et al., 2013). Such a sample would require a

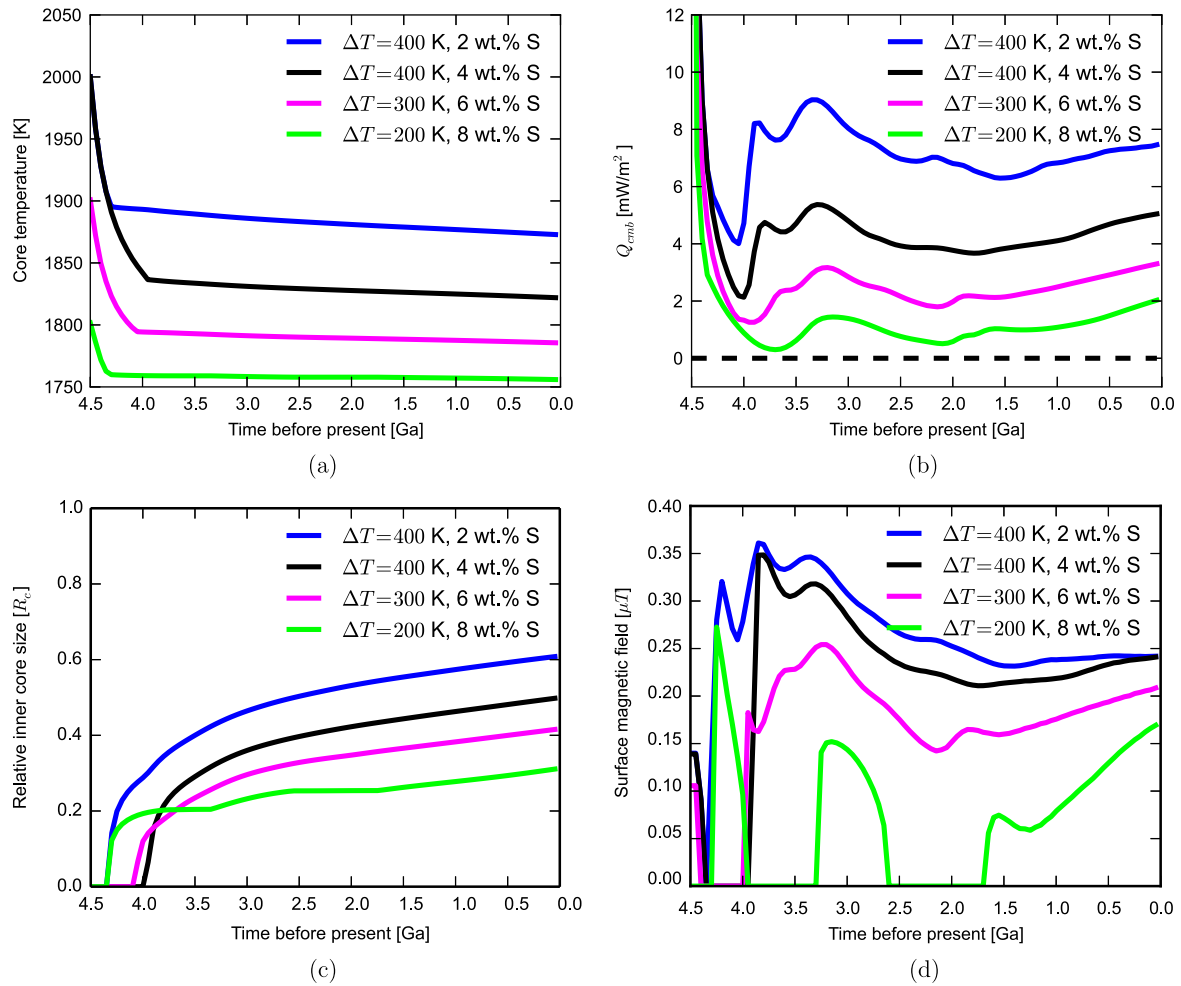


**Fig. 5.** Comparison of the outcomes for several models with different initial conditions. From top left to bottom right: (a) core temperature as a function of time, (b) core-mantle boundary heat flow, (c) relative inner-core size and (d) predicted average surface magnetic field. A summary of the outcomes of these models can be found in Table 3.

**Table 3**

List of the simulations used in this study and their final outcomes. 'Chem. dynamo onset' corresponds to the onset of the chemically-driven dynamo. Models with the subscript 'LMO200' corresponds to cases with initially colder mantles, corresponding to initial temperatures profiles following the mantle solidus for the first 200 km.

| Model           | $\Delta T$<br>K | $\chi_0$<br>wt.% | Final $r_i$<br>$R_c$ | Max field<br>$\mu\text{T}$ | Chem. dynamo onset<br>Ga ago |
|-----------------|-----------------|------------------|----------------------|----------------------------|------------------------------|
| dT200_X8        | 200             | 8                | 0.31                 | 0.27                       | 4.4                          |
| dT300_X8_LMO200 | 300             | 8                | 0.38                 | 0.26                       | 4.0                          |
| dT300_X4        | 300             | 4                | 0.51                 | 0.36                       | 4.3                          |
| dT300_X6        | 300             | 6                | 0.42                 | 0.25                       | 4.0                          |
| dT300_X6_LMO200 | 300             | 6                | 0.47                 | 0.36                       | 4.2                          |
| dT400_X2        | 400             | 2                | 0.61                 | 0.36                       | 4.4                          |
| dT400_X4        | 400             | 4                | 0.50                 | 0.35                       | 3.9                          |

dynamo driven by core-crystallization, as no other mechanism is capable of prolonging a dynamo to that date.

Using the surface magnetic field scaling law of Aubert et al. (2009), our models predict paleomagnetic surface intensities on the order of 1  $\mu\text{T}$ . This is similar to what is obtained by other dynamo models (Le Bars et al., 2011; Dwyer et al., 2011; Evans et al., in press). Nevertheless, as these studies all used similar magnetic field scaling laws, and since an order of magnitude increase in field intensity requires a three orders of magnitude difference in dissipation, this similarity should not be surprising. These low estimates are consistent with paleomagnetic studies of the sample younger than about 3.3 Ga (Tikoo et al., 2014). Nevertheless, the much larger magnetic fields (several tens of mi-

crotelas) that are inferred between 4.2 and 3.56 billion years ago (Garrick-Bethell et al., 2009; Shea et al., 2012; Tikoo et al., 2012a; Suavet et al., 2013) can not be accounted for by any current model.

As described in the previous section, a magnetic field is predicted to exist up to the present day in our simulations, which is inconsistent with observations. As observed by Williams (2009), the Moon is close to the threshold of bottom-up versus top-down crystallization. It is thus possible that at lunar pressures, depending on the initial sulfur content, a transition between the two crystallization regimes might have occurred during the Moon's history. In the top-down (i.e., Fe-snow) regime, iron crystallizes at the core mantle boundary and then sinks down to a point where it remelts, creating a growing region of stable stratification in the

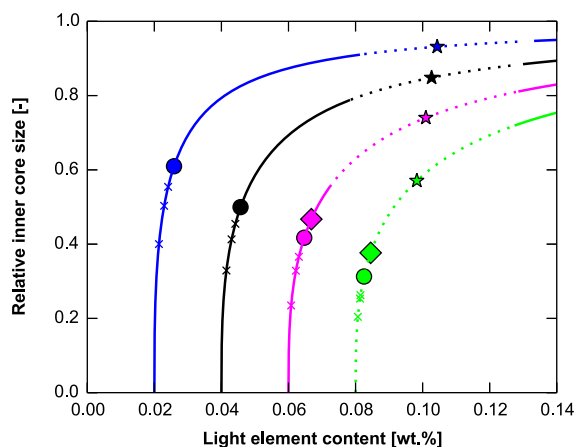


**Fig. 6.** Characterization of the transition between the bottom-up and top-down crystallization regimes. The curves correspond to possible evolutions of the inner core size and outer core light element concentration. The simulations start with no inner core on the bottom of the plot, and the colored dots show the final positions of the actual simulations. The colored crosses represent the position after 1, 2 and 3 billion years, respectively. The colored squares correspond to final positions of simulations with colder initial mantles. The colored stars are the calculated positions of the Fe–snow transition for standard parameters, and the dotted regions correspond to the range of positions of this transition within the error bars of the parameters. (For interpretation of the references to color in this figure legend, the reader is referred to the web version of this article.)

upper part of the core. Convection is still possible in the lower core, but the stably stratified region is expected to grow to the full extent of the core in less than 100 Ma (Rückriemen et al., 2014). Furthermore, during the growth of this stably stratified region, the field strengths will decrease sharply as a result of the scaling law dependence on the radius of the convecting region.

Assuming this transition would stop the compositionally-driven dynamo, we investigated its properties. In Fig. 6, the paths of inner core size and light element content of the outer core that are predicted for 4 different total core sulfur abundances are plotted. For each line, time advances forward from an inner core size of zero on the bottom of the plot, upwards. The dots represent the present day outcomes from our simulations. The transition from bottom-up crystallization to Fe–snow is defined as the point in the phase space where the liquidus and adiabat have the same average slope within the outer core. The transition points for our simulations are depicted as stars in the figure and the dotted lines represent that region of phase space where top down crystallization could occur within the uncertainties on the pressure profile and thermal expansion. Those regions depicted by solid lines always lie within the bottom-up crystallization regime. The main uncertainty in defining this transition is the lunar pressure profile. A 0.1 GPa uncertainty on the central pressure leads to a 1 wt.% difference in transition sulfur content.

This image shows that as crystallization proceeds, the abundance of light elements in the outer core increases, and we progressively approach the transition from bottom-up to top-down crystallization. For initial sulfur abundances of 2, 4, and 6 wt.%, our simulations remain entirely within the bottom-up regime, but for the simulation with 8 wt.% sulfur, it is possible that a transition from bottom-up to top-down crystallization could have occurred. Furthermore, if we were to have run our simulations further in time (as a rough approximation of colder initial conditions), we would eventually have crossed this transition.

It is important to stress that these results depend upon our assumptions on mantle evolution. If the mantle was slightly colder, or less viscous (consistent with more water content), the simulations would produce larger inner cores at present. For example, simulations with an 80 K cooler lower mantle, corresponding to an

initial temperature profile following the mantle solidus in the first 200 km, are shown as squares on Fig. 6 and produce inner cores that are about 15% larger than our nominal cases. It is therefore important for future studies to constrain this transition better.

If we were able to constrain the inner core size from other means, we could use this information to determine which sulfur abundances are required to transition from the bottom-up to top-down crystallization regimes. If the inner core is 0.7  $R_c$  in radius, as suggested by seismic data (Weber et al., 2011), then we should have entered the Fe–snow regime for cases with more than about 5 wt.% sulfur.

## 5. Conclusions

We have shown that inner core growth is a natural way to explain the long lasting lunar magnetic field. The first order result of our models is that inner core growth starts early in lunar evolution, and continues up to the present day. Inner core growth is therefore a natural and efficient way to explain a long lasting dynamo field. As standard initial conditions for lunar mantle thermal evolution lead to inner core growth for initial sulfur contents smaller than about 12 wt.%, this process should no longer be ignored when studying lunar magnetism. Given the lack of reliable paleomagnetic data between 3.56 Ga ago and the present day, if suitable lunar samples could be found, we suspect that the duration of lunar magnetic field generation might be extended considerably in time. Indeed, preliminary measurements by Tikoo et al. (2014) suggest the existence of a dynamo field younger than 3.3 Ga, and maybe as young as  $\sim 1.3$  Ga (Fagan et al., 2013). The only mechanism that is capable of explaining a dynamo at that time is core crystallization.

There are two possible scenarios to account for the apparent paradox that the Moon does not have a dynamo generated magnetic field today. Though it is possible that the Moon never crystallized a solid inner core, our simulations show that the core sulfur abundance would need to be greater than about 12 wt.%. Alternatively, we suggest that a transition between bottom-up and top-down crystallization could have occurred, as the outer core became increasingly sulfur rich. We have shown that this scenario could have occurred for initial sulfur contents between 6 and 8 wt.%.

Core sulfur abundance estimates from seismologic arguments by Weber et al. (2011) suggest that less than 6 wt.% is present in the core, while Garcia et al. (2011, 2012) argue that no significant constraint can be made when error bars are taken into account. New constraints from metal–silicate partitioning of siderophile elements also show that about 6 wt.% sulfur is expected to be present in the lunar core (Rai and van Westrenen, 2014). Independent estimates of either core sulfur content or inner core size would strongly constrain lunar thermal evolution simulations, and by consequence, the evolution of the Moon’s magnetic field. An inner-core detection scheme using GRAIL data has been proposed by Williams (2007), and other independent estimates can be obtained by future seismic data or cosmochemical modeling.

## Acknowledgements

This work was performed using the Norddeutscher Verbund für Hoch- und Höchst-leistungsrechnen (HLRN) through the project ‘Partial melting and the thermo-chemical evolution of terrestrial planets’. This work was partially funded by the UnivEarths LabEx program of Sorbonne Paris Cité (ANR-10-LABX-0023 and ANR-11-IDEX-0005-02) as well as by the Helmholtz Association through the research alliance ‘Planetary Evolution and Life.’ M. Laneuville wishes to thank S. Labrosse and S. Tikoo for the insightful discussions. The authors also wish to thank F. Nimmo and an

anonymous reviewer for their help improving this manuscript, and Y. Ricard for editorial handling.

## References

- Anderson, W.W., Ahrens, T.J., 1994. An equation of state for liquid iron and implications for the Earth's core. *J. Geophys. Res., Solid Earth* 99, 4273–4284.
- Aubert, J., Labrosse, S., Poitou, C., 2009. Modelling the palaeo-evolution of the geodynamo. *Geophys. J. Int.* 179, 1414–1428.
- Buono, A.S., Walker, D., 2011. The Fe-rich liquidus in the Fe–FeS system from 1 bar to 10 GPa. *Geochim. Cosmochim. Acta* 75, 2072–2087.
- Christensen, U.R., Aubert, J., 2006. Scaling properties of convection-driven dynamos in rotating spherical shells and application to planetary magnetic fields. *Geophys. J. Int.* 166, 97–114.
- Christensen, U.R., Holzwarth, V., Reiners, A., 2008. Energy flux determines magnetic field strength of planets and stars. *Nature* 457, 167–169.
- Cisowski, S.M., Collinson, D.W., Runcorn, S.K., Stephenson, A., Fuller, M.D., 1983. A review of lunar paleointensity data and implications for the origin of lunar magnetism. *J. Geophys. Res.* 88, A691–A704.
- Dwyer, C.A., Stevenson, D.J., Nimmo, F., 2011. A long-lived lunar dynamo driven by continuous mechanical stirring. *Nature* 479, 212–214.
- Dyal, P., Parkin, C.W., Sonett, C.P., 1970. Apollo 12 magnetometer: measurement of a steady magnetic field on the surface of the Moon. *Science* 169, 762–764.
- Evans, A.J., Zuber, M.T., Weiss, B.P., Tikoo, S.M., in press. A wet, heterogeneous lunar interior: lower mantle and core dynamo evolution. *J. Geophys. Res., Planets* 119. <http://dx.doi.org/10.1002/2013JE004494>.
- Fagan, A.L., Joy, K.H., Kring, D.A., 2013. Trapped  $^{40}\text{Ar}/^{36}\text{Ar}$  closure ages of Apollo 15 regolith samples lithified over the past 3 billion years. In: 44th Lunar and Planetary Science Conference, p. 2392.
- Fuller, M.D., Cisowski, S.M., 1987. Lunar paleomagnetism. *Geomagnetism* 2, 307–455.
- Garcia, R.F., Gagnepain-Beyneix, J., Chevrot, S., Lognonné, P., 2011. Very preliminary reference Moon model. *Phys. Earth Planet. Inter.* 188, 96–113.
- Garcia, R.F., Gagnepain-Beyneix, J., Chevrot, S., Lognonné, P., 2012. Erratum to “Very preliminary reference Moon model”. *Phys. Earth Planet. Inter.* 202–203, 89–91.
- Garrick-Bethell, I., Weiss, B.P., Shuster, D.L., Buz, J., 2009. Early Lunar magnetism. *Science* 323, 356.
- Glatzmaier, G.A., Coe, R.S., Hongre, L., Roberts, P.H., 1999. The role of the Earth's mantle in controlling the frequency of geomagnetic reversals. *Nature* 401, 885–890.
- Heimpel, M.H., Aurnou, J.M., Al-Shamali, F.M., Gomez Perez, N., 2005. A numerical study of dynamo action as a function of spherical shell geometry. *Earth Planet. Sci. Lett.* 236, 542–557.
- Hood, L.L., Richmond, N.C., Spudis, P.D., 2013. Origin of strong lunar magnetic anomalies: further mapping and examinations of LROC imagery in regions antipodal to young large impact basins. *J. Geophys. Res., Planets* 118, 1265–1284.
- Hüttig, C., Stemmer, K., 2008. Finite volume discretization for dynamic viscosities on Voronoi grids. *Phys. Earth Planet. Inter.* 171, 137–146.
- de Koker, N., Steinle-Neumann, G., Vlček, V., 2012. Electrical resistivity and thermal conductivity of liquid Fe alloys at high P and T, and heat flux in Earth's core. *Proc. Natl. Acad. Sci.* 109, 4070–4073.
- Komabayashi, T., Fei, Y., 2010. Internally consistent thermodynamic database for iron to the Earth's core conditions. *J. Geophys. Res.* 115, B03202.
- Konrad, W., Spohn, T., 1997. Thermal history of the Moon – implications for an early core dynamo and post-accretionary magmatism. *Adv. Space Res.* 19, 1511.
- Labrosse, S., 2003. Thermal and magnetic evolution of the Earth's core. *Phys. Earth Planet. Inter.* 140, 127–143.
- Laneuville, M., Wiczeorek, M.A., Breuer, D., Tosi, N., 2013. Asymmetric thermal evolution of the Moon. *J. Geophys. Res., Planets* 118, 1435–1452.
- Lawrence, D.J., Feldman, W.C., Barraclough, B.L., Binder, A.B., Elphic, R.C., Maurice, S., Thomsen, D.R., 1998. Global elemental maps of the Moon: the lunar prospector gamma-ray spectrometer. *Science* 281, 1484.
- Lawrence, K., Johnson, C., Tauxe, L., Gee, J., 2008. Lunar paleointensity measurements: implications for lunar magnetic evolution. *Phys. Earth Planet. Inter.* 168, 71–87.
- Le Bars, M., Wiczeorek, M.A., Karatekin, Ö., Cébron, D., Laneuville, M., 2011. An impact-driven dynamo for the early Moon. *Nature* 479, 215–218.
- Nimmo, F., 2007. Thermal and Compositional Evolution of the Core. *Treatise on Geophysics*, vol. 8. Elsevier, Amsterdam.
- Nimmo, F., 2009. Energetics of asteroid dynamos and the role of compositional convection. *Geophys. Res. Lett.* 36, L10201.
- Nishida, K., Terasaki, H., Ohtani, E., Suzuki, A., 2008. The effect of sulfur content on density of the liquid Fe–S at high pressure. *Phys. Chem. Miner.* 35, 417–423.
- Olson, P., Christensen, U.R., 2006. Dipole moment scaling for convection-driven planetary dynamos. *Earth Planet. Sci. Lett.* 250, 561–571.
- Purucker, M.E., Nicholas, J.B., 2010. Global spherical harmonic models of the internal magnetic field of the Moon based on sequential and coestimation approaches. *J. Geophys. Res.* 115, E12007.
- Rai, N., van Westrenen, W., 2014. Earth and planetary science letters. *Earth Planet. Sci. Lett.* 388, 343–352.
- Rückriemen, T., Breuer, D., Laneuville, M., Spohn, T., 2014. Evolution of the Moon's Core in the Fe–snow Regime. In: 45th Lunar and Planetary Science Conference, p. 2546.
- Shea, E.K., Weiss, B.P., Cassata, W.S., Shuster, D.L., Tikoo, S.M., Gattacceca, J., Grove, T.L., Fuller, M.D., 2012. A long-lived lunar core dynamo. *Science* 335, 453–456.
- Solomon, S.C., 1979. Formation, history and energetics of cores in the terrestrial planets. *Phys. Earth Planet. Inter.* 19, 168–182.
- Stegman, D.R., Jellinek, A.M., Zatman, S.A., Baumgardner, J.R., Richards, M.A., 2003. An early lunar core dynamo driven by thermochemical mantle convection. *Nature* 421, 143–146.
- Stevenson, D.J., Spohn, T., Schubert, G., 1983. Magnetism and thermal evolution of the terrestrial planets. *Icarus* 54, 466–489.
- Suavet, C., Weiss, B.P., Cassata, W.S., Shuster, D.L., Gattacceca, J., Chan, L., Garrick-Bethell, I., Head, J.W., Grove, T.L., Fuller, M.D., 2013. Persistence and origin of the lunar core dynamo. *Proc. Natl. Acad. Sci.* 110, 8453–8458.
- Takahashi, F., Tsunakawa, H., 2009. Thermal core–mantle coupling in an early lunar dynamo: implications for a global magnetic field and magnetosphere of the early Moon. *Geophys. Res. Lett.* 36, L24202.
- Tikoo, S.M., Weiss, B.P., Buz, J., Lima, E.A., Shea, E.K., Melo, G., Grove, T.L., 2012a. Magnetic fidelity of lunar samples and implications for an ancient core dynamo. *Earth Planet. Sci. Lett.* 337–338, 93–103.
- Tikoo, S.M., Weiss, B.P., Grove, T.L., Fuller, M.D., 2012b. Decline of the ancient lunar core dynamo. In: 43rd Lunar and Planetary Science Conference, p. 2691.
- Tikoo, S.M., Weiss, B.P., Shuster, D.L., Fuller, M.D., 2014. How long did the lunar core dynamo persist? In: 45th Lunar and Planetary Science Conference, p. 1972.
- Tsunakawa, H., Shibuya, H., Takahashi, F., Shimizu, H., Matsushima, M., Matsuoka, A., Nakazawa, S., Otake, H., Iijima, Y., 2010. Lunar magnetic field observation and initial global mapping of lunar magnetic anomalies by MAP-LMAG Onboard SELENE (Kaguya). *Space Sci. Rev.* 154, 219–251.
- Weber, R.C., Lin, P.Y., Garnero, E.J., Williams, Q., Lognonné, P., 2011. Seismic detection of the lunar core. *Science* 331, 309–312.
- Wiczeorek, M.A., Jolliff, B.L., Khan, A., Pritchard, M.E., Weiss, B.P., Williams, L.L., Hood, L.L., Richter, K., Neal, C.R., Shearer Jr, C.K., McCallum, I.S., Tompkins, S., Hawke, B.R., Peterson, C.A., Gillis-Davis, J.J., Bussey, D.B.J., 2006. The constitution and structure of the lunar interior. In: *New Views of the Moon*. Mineralogical Society of America.
- Williams, J.G., 2007. A scheme for lunar inner core detection. *Geophys. Res. Lett.* 34, L03202.
- Williams, J.G., Boggs, D.H., Yoder, C.F., Ratcliff, J.T., Dickey, J.O., 2001. Lunar rotational dissipation in solid body and molten core. *J. Geophys. Res.* 106, 27933–27968.
- Williams, Q., 2009. Bottom-up versus top-down solidification of the cores of small solar system bodies: constraints on paradoxical cores. *Earth Planet. Sci. Lett.* 284, 564–569.
- Zhang, N., Parmentier, E.M., Liang, Y., 2013. A 3D numerical study of the thermal evolution of the Moon after cumulate mantle overturn: the importance of rheology and core solidification. *J. Geophys. Res., Planets* 118, 1–16.